Spectrochimica Acta Part A: Molecular and Biomolecular Spectroscopy 239 (2020) 118530

Contents lists available at ScienceDirect

Spectrochimica Acta Part A: Molecular and Biomolecular Spectroscopy

journal homepage: www.elsevier.com/locate/saa

Probing the structure-function relationship of hemoglobin in living human red blood cells

Jakub Dybas [a,b], Matthew J. Bokamper [a], Katarzyna M. Marzec [b,*], Piotr J. Mak [a,*]

[a] Saint Louis University, Chemistry Department, 3501 Laclede Ave., 63103 Saint Louis, MO, United States
[b] Jagiellonian University, Jagiellonian Centre for Experimental Therapeutics (JCET), 14 Bobrzyńskiego Str., 30–348 Krakow, Poland

ARTICLE INFO

Article history:
Received 12 February 2020
Received in revised form 14 May 2020
Accepted 22 May 2020
Available online 29 May 2020

Keywords:
Resonance Raman spectroscopy (RR)
Red blood cells (RBCs)
Hemoglobin (Hb)
Structure-function relationship

ABSTRACT

Hemoglobin (Hb) is a key component of respiratory system and as such plays important role in human physiology. The studies of Hb's structure and functions are usually performed on cell-free protein; however, it has been shown that there are functionally relevant differences between isolated Hb and Hb present inside red blood cells (RBCs). It is clear that new experimental approaches are needed to understand the origin of these differences and to gain insight into the structure-function relationship of Hb within intact living cells. In this work we present a novel application of Resonance Raman spectroscopy to study heme active site of different forms of human Hb within living RBCs using laser excitation lines in resonance with their Soret absorption bands. These studies revealed that there are no significant changes in the disposition of the Fe-O-O fragment or the Fe-N_{His} linkage for Hb molecules enclosed in RBCs and these in free isolated states. However, some changes in the orientation of the heme vinyl groups were observed which might account for the differences in the protein activity and ligand affinity. This work highlights importance of protein-based studies and presents a new opportunity to translate these results to physiological cell systems.

1. Introduction

Hemoglobin (Hb) is a key heme protein in red blood cells (RBC) and constitutes up to 95% of the protein content in erythrocytes [1–3]. It is a subject of extensive research not only because of its key function in aerobic respiration but also because it is an important model for allosteric regulation and cooperative oxygen binding [1]. Adult human hemoglobin (97% of Hb A1 and 3% of Hb A2) is a tetramers composed of four subunits, two identical α subunits and two identical β subunits made of 141 and 146 amino acid residues, respectively; each subunit contains one prosthetic group, iron protoporphyrin IX, or heme *b* [1,4]. While Hb transports oxygen and maintains acid-base balance with deoxyhemoglobin (deoxyHb) and oxyhemoglobin (oxyHb) serving as an acceptors and donors of oxygen molecules, respectively, recent studies indicate its important roles in bioavailability of other gaseous molecules, such as nitric oxide [1,3,5]. The great majority of all human Hb in functional erythrocytes exist in ferric oxy form (oxyHb) and ferrous deoxy form constituting approximately up to 97–98% of all Hb forms with their relative ratio depending on the blood type (arterial vs venous) [1,5–7]. Methemoglobin (metHb), a ferric form of Hb unable to bind oxygen, is generated in RBCs due to the auto-oxidation of oxygenated Hb and is continuously reduced by cytochrome b_5 reductase (metHb reductase) in functional RBCs, and therefore its level in erythrocytes does not exceed 1% under healthy conditions [1,8,9]. Other Hb species present inside RBCs are carboxyhemoglobin (HbCO) and sulfohemoglobin (Hb–SH_2) constituting about 0.4–1.5% and up to 0.4% of the total Hb content, respectively [7].

The majority of the Hb studies are performed on free Hb isolated from RBCs and dispersed in buffer solutions. However, the isolated Hb protein and Hb molecules enclosed within RBCs exhibit biologically relevant differences such as changes in activity or ligand affinity [10–12]. The RBCs' internal environment ensures safe Hb confinement where the cell's membrane and cytoskeleton, together with unstirred layer of surrounding plasma, create barriers which decrease the affinity of gaseous molecules to Hb molecules [13,14]. Moreover, there is significantly larger degree of molecular crowding in erythrocytes as compared to Hb in solution; e.g., due to the tight packing, tetrameric Hb molecule within RBCs reaches the concentration of around 5 mM, much higher than it's possible to obtain by dissolving cell-free protein [15]. It was even suggested, that ordering of Hb molecules within RBCs might resemble a semi-crystalline state, typical for a solid rather than that of dissolved Hb [16]. The higher ordering and tight packing of Hb molecules as well as modified orientation of heme groups in Hb enclosed within RBCs were also postulated to lead to an enhancement of Raman signal with the use of laser excitation far from the electronic transition energy [16,17]. This off-Resonance enhancement allowed studies of some Hb

* Corresponding authors.
E-mail addresses: katarzyna.marzec@jcet.eu (K.M. Marzec), piotr.mak@slu.edu (P.J. Mak).

https://doi.org/10.1016/j.saa.2020.118530

adducts in functional RBCs including Hb-NO [18], Hb-NO_2^- [19] as well as degraded Hb species inside Kupffer cells and macrophages [20]. However, the detailed comparison between Hb adducts observed inside RBC and in isolated form obtained in the same conditions, have not been reported before.

While many techniques, including X-ray crystallography, allow studies of the isolated proteins and provide precise information about their molecular structures, this level of structural insight into proteins enclosed within functional cells is often impossible. The classical techniques used in RBCs analysis, such as flow cytometry, serology or histological staining, are focused on RBC membrane proteins detection instead of characterization of encapsulated Hb molecules [1,21]. The electronic absorption spectroscopy, commonly used in medicine for blood gas analysis, allows differentiating between some forms of Hb, but often lacks of specificity and needed structural insight on the molecular level [1,18]. On the other hand, Resonance Raman spectroscopy (RR) and microspectroscopy have been successfully and extensively used in studies of isolated and RBC-enclosed hemoglobin [17–19,22–27]. The RR was shown to provide a great deal of information on heme active site structure and its relationship to protein function. More specifically, in the high frequency spectral region, heme marker modes respond to changes in oxidation- or spin-state of the central heme iron in well-established ways [28–30]. In the low frequency region the RR modes document changes in heme planarity and in protein interactions with heme periphery, such as vinyl and propionate groups. It is important to monitor these changes because the alterations in heme planarity or presence of potentially conjugated vinyl or propionic acid peripheral substituents have important functional consequences; e.g., they are considered as effective structural determinants of heme reactivity [31,32]. The RR is also a remarkably effective probe of the key linkages between the heme prosthetic group and its endogenous and exogenous ligands; i.e., it is possible to efficiently enhance internal modes of the Fe-N_{His} linkage or modes associated with the Fe-XY fragments, where XY indicates a exogenous ligands such as O_2, CO, CN^-, etc. [33–36]. The iron-protein linkage have obviously great impact on heme reduction potential and exogenous ligands binding affinities while the information regarding the disposition of Fe-X-Y linkage has direct relevance to protein reactivity. The structure-function studies of Hb inside intact living cells are more challenging due to experimental restrictions. Currently, an application of Raman microspectroscopy with off-resonance and Q-band resonance excitation laser lines allowed successful differentiation between deoxygenated and oxygenated states and monitoring effects of different stressors on the Hb oxygenation state. The application of RR spectroscopy to study Hb structures within intact RBC has an enormous potential for clinical applications, e.g., detection of hemozoin can be used in malaria diagnostic. Furthermore, RR technique can be used in monitoring of oxygen saturation or methemoglobin levels, as well as to study RBCs disorders such as thalassemia or sickle-cell disease [27,37–39]. However, until now, no RR excitation within the maximum of Soret absorption bands was applied to probe heme active site environment of Hb for functional erythrocytes, the successful implementation of this approach could allow more sophisticated and novel clinical applications.

In this work we study structures of Hb molecules enclosed within RBCs in comparison with the isolated proteins in buffer solution. We characterized metHb, deoxyHb and oxyHb adducts (for molecular structure of their heme moieties please see Fig. 1) using UV–Vis electronic absorption and RR, the later within resonance with corresponding Soret bands. Moreover, we carried out isotope sensitive experiments with the use of $^{16}O_2$ and $^{18}O_2$ isotopes in order to detect and probe the disposition of the Fe-O-O fragment of oxyHb adducts inside RBCs and to characterize their Raman spectral patterns. Careful comparison of the Soret enhanced RR spectra of met-, deoxy- and oxy- forms of Hb enclosed within RBCs with corresponding isolated Hbs in solutions reveals unique insight into the differences between their heme active sites and sheds new light into the impact of the cell environment on Hb molecular structures. Presented herein data show that while the studies of isolated proteins are crucial for structure-function research, the studies of proteins in situ, e.g. Hb enclosed within RBCs are needed for better understanding of their structure function relationship.

2. Materials and methods

2.1. Chemicals and solutions

Sodium chloride was purchased from Fisher Scientific (Hampton, NH, USA) and sucrose from Bio Basic (Markham ON, Canada). Sodium nitrite and sodium dithionate were purchased from Sigma-Aldrich (Saint Louis, MO, USA). The human RBCs were purchased from the Interstate Blood Bank, Inc. (Memphis, TN, USA). RBCs were washed and stored in 0.9% sodium chloride solution supplemented with 0.2% sucrose and the pH of the solution was adjusted to 7.4 using 1 M hydrochloric acid to keep the cells under functional conditions.

2.2. Sample preparation

2.2.1. Preparation of RBCs for the RR and UV–Vis measurements

The human RBCs were washed by triple centrifugation process (acceleration: 800 ×*g*; run time: 5 min; temperature: 4 °C) with 0.9% sodium chloride solution supplemented with 0.2% sucrose and pH 7.4. The supernatant and the buffy coat were removed by aspiration after each spin. RBCs were then suspended in the same solution to give hematocrit (Hct) of approximately 0.1% corresponding to about 5 μM of Hb tetramer (20 μM relating to single Hb subunit).

2.2.2. Isolation of human Hb from RBCs for the RR and UV–Vis measurements

RBCs were diluted 1:1 (v/v) with 0.9% saline and subjected to triple centrifugation (acceleration: 8000 ×*g*; run time: 15 min; temperature: 4 °C) followed each time be removal of supernatant and buffy coat. After fourth centrifugation, RBCs were diluted 1:4 (v/v) with cold deionized water (4 °C) and then incubated for 30 min in 4 °C. The lysed cells were centrifuged at 23000 ×*g* for 90 min (4 °C) to remove cell debris. The Hb-containing supernatant was aspirated and the Hb concentration was measured using UV–Vis absorption spectroscopy and estimated to be around 1.25 mM per tetramer. The concentration of Hb for RR and

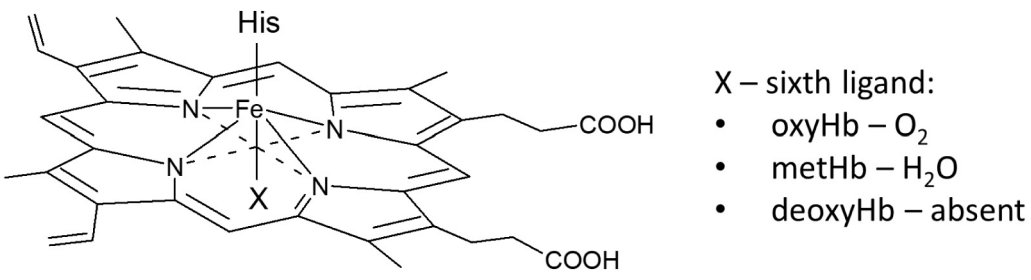

Fig. 1. Molecular structure of the heme moieties of studied Hb adducts.

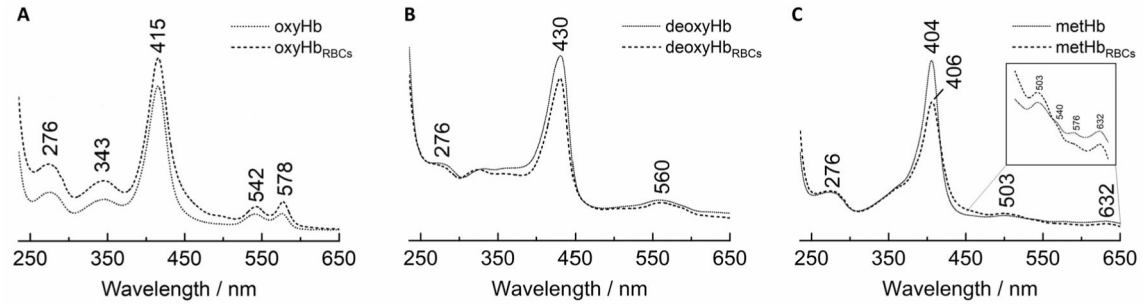

Fig. 2. UV–Vis absorption spectra of oxy adducts (A), ferrous (B) and ferric (C) isolated Hb species (solid line) compared with the corresponding spectra of Hb enclosed within RBCs. The inset presented in the C panel corresponds to the extended 450–650 nm wavelength region.

Table 1
The summary of electronic absorption bands (nm) of various Hb species as isolated protein and inside functional human RBCs.

	Soret Isolated/in RBC	Q_{IV} Isolated/in RBC	Q_v Isolated/in RBC	Q_0 Isolated/in RBC	CT Isolated/in RBC
oxyHb	415/415	–	542/542	578/578	–
deoxyHb	430/430	–	560/560		–
metHb	404/406	503/503	540/540	576/576	632/632

UV–Vis measurements was approximately 12.5 μM of Hb tetramer (50 μM in heme).

2.2.3. Preparation of various forms of Hb

The Hb protein isolated form RBCs is in oxy form. The reduction of oxyHb to deoxyHb was achieved by anaerobic addition of freshly prepared sodium dithionate in a 10-fold molar excess. To generate the metHb, the isolated oxyHb was incubated with 1.2 M excess of potassium ferricyanide(III) followed by purification using size-exclusion chromatography column (Bio-Gel P-6, BioRad). The functional RBCs samples were exposed to air for about an hour to ensure full oxygenation of the enclosed Hb protein. As in case with isolated Hb, the deoxy form was prepared by addition of $Na_2S_2O_4$ under anaerobic conditions. To obtain metHb, RBCs were pretreated with $NaNO_2$ (10 mM) for 15 min at room temperature, followed by buffer exchange.

2.3. Data acquisition

2.3.1. Resonance Raman spectroscopy (RR)

The RR spectra of met and oxy adducts of isolated Hb and Hb inside of RBC were measured using 406.7 and 413.1 nm excitation lines respectively, from Innova 302C Kr^+ laser (Coherent Inc.), while the deoxy samples were excited using 441.6 nm laser line from a He-Cd laser (Kimmon Koha, Co.). The RR data were acquired using 1250 M-Series II high-resolution spectrometer (Horiba, Ltd.) equipped with a liquid nitrogen cooled PyLoN:400B CCD detector (Princeton Instrument, NJ). Measurements were done using a 180° backscattering geometry and the laser beam was focused onto the sample using a cylindrical lens. The laser power at the sample was adjusted to approximately 1 mW for measurements of oxy samples, in order to avoid any oxygen photodissociation [24], and 5 mW for measurements of met and deoxy forms. All measurements were conducted at room temperature. The slit width was set at 150 μm and the 1200 g/mm grating was used and the spectral resolution was equal to 1.5 cm^{-1}. The size of the laser spot on the samples was approximately 1.0 mm × 0.1 mm for 406 nm and 413 nm excitation lines and approximately 2.0 mm × 0.2 mm in

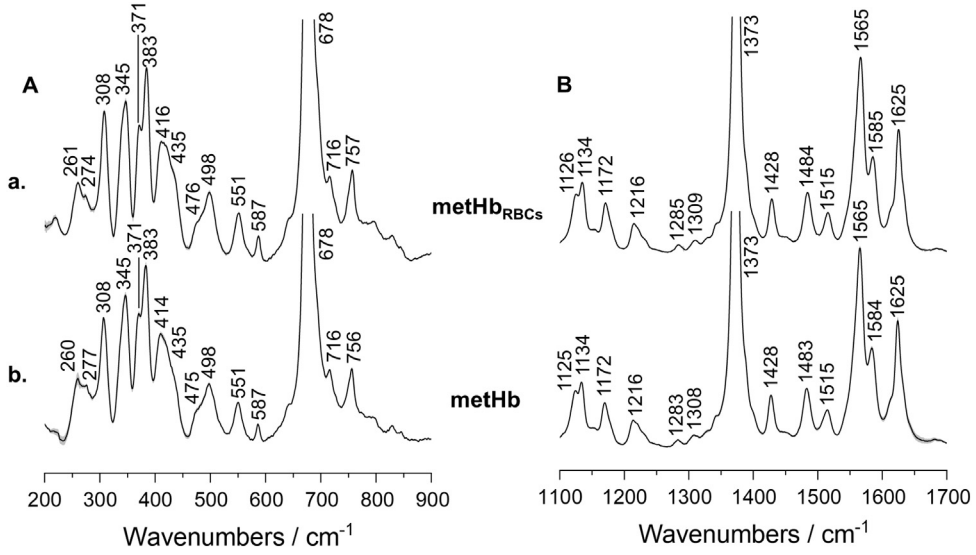

Fig. 3. RR spectra of metHb (ferric Hb specie) for proteins enclosed within RBCs (a, $metHb_{RBCs}$) and isolated (b, metHb). Spectra were recorded with 406 nm excitation lines and are presented in the low (A, 200–900 cm^{-1}) and medium (B, 1100–1700 cm^{-1}) wavenumber regions. All spectra were averaged from 3 independent experiments from 9 single spectra in total (3 spectra per experiment). Acquisition time was equal to 5 min per spectrum (10 s and 30 accumulations) in case of low frequency region (A) and 3 min per spectrum (10 s and 18 accumulations) in case of medium frequency region (B). All averaged RR spectra are presented with their standard deviation (SD).

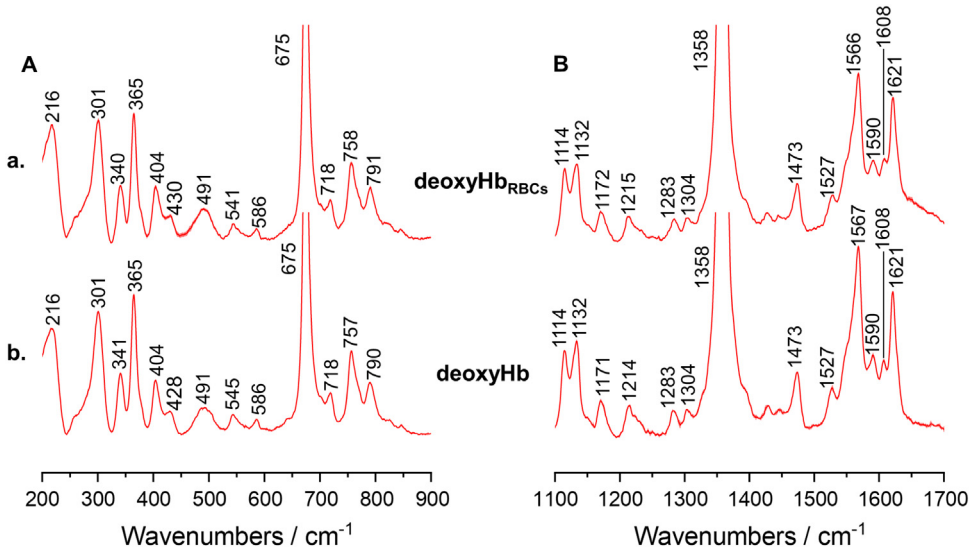

Fig. 4. RR spectra of deoxyHb (ferrous Hb specie) for proteins enclosed within RBCs (a, deoxyHb$_{RBCs}$) and isolated (b, deoxyHb). Spectra were recorded with 442 nm excitation lines and are presented in the low (A, 200–900 cm^{-1}) and medium (B, 1100–1700 cm^{-1}) wavenumber regions. All spectra were averaged from 3 independent experiments from 9 single spectra in total (3 spectra per experiment). Acquisition time was equal to 5 min per spectrum (10 s and 30 accumulations) in case of low frequency region (A) and 3 min per spectrum (10 s and 18 accumulations) in case of medium frequency region (B). All averaged RR spectra are presented with their standard deviation.

case of 442 nm excitation line. The samples were placed in 5 mm OD NMR tubes and spun to avoid local heating and ligand photodissociation as well as to average obtained signal from the whole sample volume.

Table 2
Wavenumbers (cm^{-1}) for the most prominent Raman bands with assignments and local coordinates for metHb and deoxyHb adducts formed inside RBCs or with the use of isolated Hb protein [25,30,40,41,43–45].

Band	Local coordinate	Wavenumber/cm^{-1}			
		metHb$_{RBCs}$	metHb	deoxyHb$_{RBCs}$	deoxyHb
	ν(Fe—His)	–	–	216$_m$	216$_m$
ν_9	$\delta(C_\beta C_1)_{sym}$	261$_w$	260$_w$	–	–
ν_{52}	$\delta(C_\beta C_1)_{sym}$	274$_{sh}$	277$_{sh}$	–	–
γ_7	$\gamma(C_\alpha C_m)$	308$_m$	308$_m$	301$_m$	301$_m$
ν_8	ν(Fe—N)	345$_m$	345$_m$	340$_m$	341$_m$
COO$^-$	$\delta(C_\beta C_c C_d)$	371$_{sh}$	371$_{sh}$	365$_m$	365$_m$
COO$^-$	$\delta(C_\beta C_c C_d)$	383$_m$	383$_m$	–	–
4-vinyl	$\delta(C_\beta C_a C_b)$	416$_m$	414$_m$	404$_m$	404$_m$
2-vinyl	$\delta(C_\beta C_a C_b)$	435$_{sh}$	435$_{sh}$	430$_{sh}$	428$_{sh}$
ν_{33}	$\delta(C_\alpha C_\beta C_\beta)$	476$_{sh}$	475$_{sh}$	476$_{sh}$	475$_{sh}$
γ_{12}	(pyr swiv)	–	–	491$_m$	491$_m$
	$\nu(Fe–OH)_{HS}$	498$_m$	498$_m$	–	–
γ_{21}	$(pyr\ fold)_{sym}$	551$_w$	551$_w$	541$_w$	545$_w$
ν_{48}	$\delta(pyr\ def)_{sym}$	587$_w$	587$_w$	586$_w$	586$_w$
ν_7	$\delta(pyr\ def)_{sym}$	678$_s$	678$_s$	675$_s$	675$_s$
γ_{11}	$(pyr\ fold)_{as}$	716$_{sh}$	716$_{sh}$	718$_{sh}$	718$_{sh}$
ν_{15}	ν(pyr br)	757$_m$	756$_m$	758$_m$	757$_m$
ν_6	$\delta(C_\alpha C_m C_\alpha)$	–	–	791$_m$	790$_m$
ν_5	$\nu(C_\beta$–methyl)	1126$_m$	1125$_m$	1114$_m$	1114$_m$
ν_{22}	$\nu(pyr\ hr)_{as}$	1134$_m$	1134$_m$	1132$_m$	1132$_m$
ν_{30}	$\nu(pyr\ hr)_{as}$	1172$_m$	1172$_m$	1172$_m$	1171$_m$
$\nu_5/\nu_{13}/\nu_{42}$	$\delta(C_m H)$	1216$_m$	1216$_m$	1215$_m$	1214$_m$
ν_4	$\nu(pyr\ hr)_{sym}$	1373$_{vs}$	1373$_{vs}$	1358$_{vs}$	1358$_{vs}$
ν_{28}	$\nu(C_\alpha C_m)_{sym}$	1428$_m$	1428$_m$	–	–
ν_3	$\nu(C_\alpha C_m)_{sym}$	1484$_m$	1483$_m$	1473$_m$	1473$_m$
ν_{38}	$\nu(C_\beta C_\beta)$	1515$_m$	1515$_m$	1527$_m$	1527$_m$
ν_2	$\nu(C_\beta C_\beta)$	1565$_s$	1565$_s$	1566$_s$	1567$_s$
ν_{37}	$\nu(C_\alpha C_m)_{as}$	1585$_m$	1584$_m$	1590$_m$	1590$_m$
ν_{10}	$\nu(C_\alpha C_m)_{as}$	–	–	1608$_{sh}$	1608$_{sh}$
	ν(C=C)	1625$_s$	1625$_s$	1621$_s$	1621$_s$

The mode notation is based on that proposed by Abe et al. [43] and Hu et al. [40].
ν – stretching, δ – bending, γ – out-of-plane, def – deformation, br – breathing, hr – half-ring, as – asymmetric, sym – symmetric, pyr – pyrrole; swiv – swivelling; fold – folding; w – weak; m – medium; s – strong, vs – very strong; sh – shoulder.

The presented here RR data are averaged from at least 3 independent experiments and each experiment comprised measurements and averaging of at least three individual RR spectra. The individual spectra were carefully inspected to ensure sample integrity by monitoring their spectral patterns and relative intensities of major modes, e.g., the sample did not undergo accidental photodissociation or thermal degradation during RR measurements. Spectra were calibrated using fenchone (Sigma-Aldrich, WI) and processed with Grams/32 AI software (Galactic Industries, Salem, NH) and OriginPro 2018 (OriginLab, Northampton, Massachusetts, USA). Spectra were post-processed (cosmic spike removal with median filter 3 × 3, background subtraction with asymmetric least squares method) and normalized using z-scores in whole spectral region (200–1700 cm^{-1}).

2.3.2. UV–Vis absorption spectroscopy

UV–Vis electronic absorption spectra of all the samples studied here were obtained on a Cary 60 UV–Vis spectrophotometer (Agilent Technologies, Santa Clara, CA, USA) in the range of 200–700 nm using a cuvette of 1 cm path length. The presented here UV–Vis spectra were measured at least three times for independently prepared samples followed by careful inspection of their spectral profiles to ensure samples integrity and accuracy of the data.

3. Results and discussion

3.1. Hb species characterized by UV–Vis absorption spectroscopy

The electronic absorption spectra of heme proteins are characterized by a strong band located at around 400–440 nm, called Soret band (or B band), up to four weaker Q bands between 480 and 600 nm range and an additional charge-transfer (CT) band present in high spin (HS) species at around 600–650 nm [19,22,26]. Fig. 2 shows comparison of the UV–Vis spectra of various Hb species within RBCs with the corresponding spectra of isolated proteins. The UV–Vis spectra of oxygenated forms are dominated by the Soret band at 415 nm and contain two Q bands at 542 nm and 578 nm. The spectra of ferrous Hb inside the RBS and isolated Hb exhibit Soret bands at 430 nm and single Q bands at around 560 nm. Ferric Hb species inside functional RBCs was obtained by treatment of oxyHb$_{RBCs}$ with $NaNO_2$ (10 mM) which resulted in rapid formation of the metHb as evidenced by the Soret band located at 406 nm and

four additional bands, three Q bands at 503 nm, 542 nm and 576 nm, as well as the fourth CT band located at 632 nm [18,19,24]. The UV–Vis spectra of oxy and deoxy Hb forms enclosed in the RBS and that of isolated proteins exhibit virtually identical spectral patter, while the spectrum of metHb inside RBC is two wavenumbers red shifted as compared to the spectrum of isolated metHb. It is noted that in all cases there are some slight changes in the absorption intensities of the Soret bands between isolated and RBC enclosed proteins associated most probably with the presence of the cell membrane in the RBCs which may give rise to slight alterations in the UV–Vis spectral patterns. The positions of UV–Vis bands of all Hb forms are summarized in Table 1.

3.2. Resonance Raman spectroscopy of Hb derivatives

3.2.1. Ferric and ferrous Hb

The RR spectra of metHb enclosed in RBCs (trace a) and in the solution isolated state (trace b) are shown in Fig. 3. The high frequency spectra of both proteins look identical (Fig. 3, right) with the ν_4 oxidation state marker and the ν_3 spin state marker being observed at 1373 cm^{-1} and 1485 cm^{-1}, respectively; indication of the ferric, six coordinated, high spin species. In the low frequency region, the dominant ν_7 mode is seen for both isolated and RBCs Hb, at 678 cm^{-1} and there are no changes in the frequency of the ν_8 mode at 345 cm^{-1} or two propionate bending modes seen at 371 cm^{-1} and 383 cm^{-1} (Fig. 3, left). There are two vinyl bending modes in the spectrum of the RBCs Hb observed at 416 cm^{-1} and 435 cm^{-1}, the lower frequency one being usually associated with in-plane orientation while the higher frequency one with the out-of-plane orientation of the vinyl group [34,40,41]. The in-plane vinyl bending mode in the RBC is upshifted by 2 cm^{-1} with respect to the corresponding mode seen in the spectrum of isolated Hb that is observed at 414 cm^{-1}, indicating that the higher degree of protein packing in the RBC leads to slight out-of-plane displacement of the one of the vinyl group.

The RR spectra of deoxyHb are shown in Fig. 4. There are no differences in the high frequency region between the spectra obtained for isolated and RBCs enclosed proteins. They ν_4 and the ν_3 modes are seen in both cases at the 1358 cm^{-1} and 1473 cm^{-1}, characteristic for the ferrous, five coordinated, high spin species. In the low frequency region the spectra of both isolated and RBCs deoxyHb are very similar, with the ν_7 and ν_8 modes at 675 cm^{-1} and 340 cm^{-1}, respectively. These spectra also consist of series of the heme out-of-plane modes with the intense γ_7 mode at 301 cm^{-1}. The 365 cm^{-1} propionate bending mode is also not affected changes in both proteins. Interestingly, however, small changes are noted in the disposition of the vinyl bending modes. While the lower frequency in-plane vinyl bending modes are not affected, the out-of-plane vinyl bending mode seen in the isolated

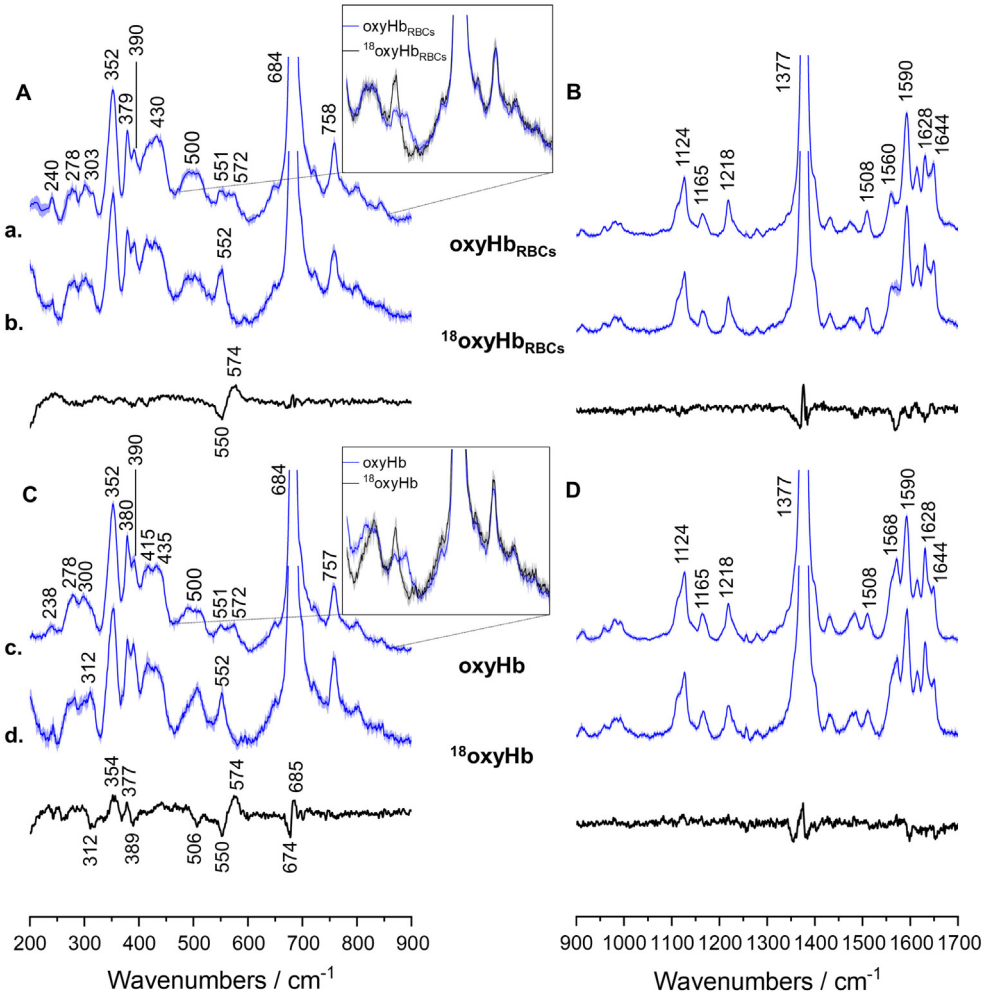

Fig. 5. RR spectra of oxyHb and ^{18}O-substitituted oxyHb for proteins enclosed within RBCs (a–b, oxyHb$_{RBCs}$) and isolated (c–d, oxyHb). Spectra were recorded with 413 nm excitation lines and are presented in the low (A and C, 200–900 cm^{-1}) and medium (B and D, 900–1700 cm^{-1}) wavenumber regions. All spectra were averaged from 3 independent experiments from 12 single spectra in total (4 spectra per experiment). Acquisition time was equal to 5 min per spectrum (10 s and 30 accumulations) in case of low frequency region (A) and 3 min per spectrum (10 s and 18 accumulations) in case of medium frequency region (B). All averaged RR spectra are presented with their standard deviation. The insets in A and C panels correspond to the expanded area in the 450–850 cm^{-1} spectral range.

deoxyHb at 428 cm^{-1} is being further moved out-of-plane in the spectrum of deoxyHb enclosed in RBCs, as seen by its upshift to higher frequency by 2 cm^{-1}. In the ferrous form, the RR is capable of directly monitoring the status of the Fe-N_{His} linkage in the histidine ligated heme proteins; the ν(Fe—N) mode for neutral histidine imidazole ligand, as in Hb molecule, being observed typically near 220 cm^{-1}. This important mode reflects changes in the Fe-N_{His} bond strength which have key impact on heme reduction potential and binding of transaxial ligands. Careful comparison of the isolated and RBC deoxyHb show that the ν(Fe—N_{His}) stretching mode is observed at 216 cm^{-1}; e.g., the crowding of the Hb molecules in the erythrocytes has no impact on this functionally important Fe-N_{His} linkage.

The peak positions of all observed modes for ferric and ferrous Hb adducts were summarized and presented in the Table 2.

3.2.2. Hb oxy adducts

The reversible binding of oxygen molecule to a ferrous deoxyHb generates ferrous dioxygen (Fe^{II}-O_2) adduct of oxyHb, which is more correctly represented by its resonance formulation of a ferric superoxide specie (Fe^{III}-O_2^-) [28,42]. The Fe-O-O fragment is inherently bend and in histidine ligated proteins is relatively stable. Since it interacts with the distal heme pocket polar molecules and can be affected by the steric interaction with the non-polar groups, the frequencies of associated modes can be very informative of the heme pocket environment allowing better understanding of the active site structural elements that control the globin's functions. The RR spectra of imidazole ligated proteins usually allow detection of only ν(Fe—O) stretching mode; e.g., the ν(O—O) mode is usually not enhanced unless the Fe-O-O fragment experience significant deformation caused by the steric or polar interactions.

The high frequency RR spectra of isolated (Fig. 5, right bottom) and RBC enclosed (right top) oxyHb are indicative of the ferric (ν_4 mode at 1377 cm^{-1}) and low spin species (the ν_3 mode at 1508 cm^{-1}), as expected [18,28,30]. The corresponding low frequency spectra are shown on the left side of Fig. 5 revealing, once again, quite similar spectral patterns between isolated and RBC Hb. While there are no differences in the ν_7 and ν_8 modes or modes associated with the propionate bending modes, it is noted that the disposition of the frequencies of vinyl bending modes are different between oxyHb molecules in isolate state and the enclosed in RBCs. The higher frequency vinyl bending mode is being observed at 435 cm^{-1} in isolated Hb samples and it shifts down to 430 cm^{-1} in the RBC enclosed in the RBCs, meaning that the presumed Hb molecules crowding in cells results in the forcing the out-of-plane vinyl group more into plane geometry.

Since the modes associated with the Fe-O-O fragment often overlap with the heme modes causing their assignment and identification difficult, the isotopic substitution of the $^{16}O_2$ to $^{18}O_2$ is often used to derive $^{16}O_2$—$^{18}O_2$ difference traces that allow easy identification of the ν(Fe—O) and ν(O—O) stretching modes. The $^{16}O_2$ and $^{18}O_2$ spectra in the low frequency region (Fig. 5, bottom left) shows that the mode ν(Fe—O) mode in isolated Hb is seen at 571 cm^{-1} and shifts to 552 cm^{-1} upon $^{18}O_2$ isotopic exchange. Similar spectral patterns are seen in samples of oxyHb enclosed in RBCs, indicating that the Fe-O-O fragment is not affected by the molecular crowding in cells; this observation is further confirmed by the inspection of the $^{16}O_2$—$^{18}O_2$ difference traces. It is noted that in the high frequency spectral region there is no enhancement of the ν(O—O) stretching modes, for neither the isolated Hb, as expected, nor the Hb in RBCs. While one could presume that the higher molecular packing in the cells might result in exertion of extra forces inducing bending of the Fe-O-O fragment. The deformation of the Fe-O-O fragment usually result in enhancement of the ν(O—O) stretching mode, however, no oxygen sensitive modes were observed in the spectra of the $oxyHb_{RBCs}$, indicating no steric (or polar) induced effects on the oxyHb enclosed in RBCs.

The peak positions of all observed modes for oxyHb and ^{18}oxyHb adducts were summarized and presented in the Table 3.

Table 3
Wavenumbers (cm^{-1}) for the most prominent Raman bands with assignments and local coordinates for oxyHb and ^{18}oxyHb adducts formed inside RBCs or with the use of isolated Hb protein [25,30,40,41,43–45].

Band	Local coordinate	Wavenumber/cm^{-1}			
		$oxyHb_{RBCs}$	oxyHb	$^{18}oxyHb_{RBCs}$	^{18}oxyHb
ν_9	$\delta(C_\beta C_1)_{sym}$	240_w	238_w	240_w	238_w
ν_{52}	$\delta(C_\beta C_1)_{sym}$	278_m	278_m	278_m	278_m
γ_7	$\gamma(C_\alpha C_m)$	303_m	300_m	303_m	300_m
ν_8	ν(Fe—N)	352_m	352_m	352_m	352_m
COO^-	$\delta(C_\beta C_c C_d)$	379_m	380_m	379_m	380_m
COO^-	$\delta(C_\beta C_c C_d)$	390_{sh}	390_{sh}	390_{sh}	390_{sh}
4-vinyl	$\delta(C_\beta C_a C_b)$	430_m	415_{sh}	430_m	415_{sh}
2-vinyl	$\delta(C_\beta C_a C_b)$	430_m	435_{sh}	430_m	435_{sh}
ν_{33}	$\delta(C_\alpha C_\beta C_\beta)$	476_{sh}	475_{sh}	476_{sh}	475_{sh}
γ_{12}	(pyr swiv)	500_m	500_m	500_m	500_m
γ_{21}	(pyr fold)$_{sym}$	551_w	551_w	ov	ov
	ν(Fe—O_2)	572_w	572_w	$552_{w/m}$	$552_{w/m}$
ν_7	δ(pyr def)$_{sym}$	684_s	684_s	684_s	684_s
ν_{15}	ν(pyr br)	758_m	757_m	758_m	757_m
ν_{22}	ν(pyr hr)$_{as}$	1124_m	1124_m	1124_m	1124_m
ν_{30}	ν(pyr hr)$_{as}$	1165_m	1165_m	1165_m	1165_m
$\nu_5/\nu_{13}/\nu_{42}$	$\delta(C_mH)$	1218_m	1218_m	1218_m	1218_m
ν_4	ν(pyr hr)$_{sym}$	1377_{vs}	1377_{vs}	1377_{vs}	1377_{vs}
ν_3	$\nu(C_\alpha C_m)_{sym}$	1508_m	1508_m	1508_m	1508_m
ν_{11}	$\nu(C_\beta C_\beta)$	1560_m	1568_m	1560_m	1568_m
ν_2	$\nu(C_\beta C_\beta)$	1590_s	1590_s	1590_s	1590_s
	ν(C=C)	1628_s	1628_s	1628_s	1628_s
ν_{10}	$\nu(C_\alpha C_m)_{as}$	1644_s	1644_s	1644_s	1644_s

The mode notation is based on that proposed by Abe et al. [43] and Hu et al. [40].
ν – stretching, δ – bending, γ – out-of-plane, def – deformation, br – breathing, hr – half-ring, as – asymmetric, sym – symmetric, pyr – pyrrole; swiv – swivelling; fold – folding; w – weak; m – medium; s – strong, vs – very strong; sh – shoulder, ov – overlapped.

4. Conclusions

The Soret enhanced RR spectra of Hb in situ RBCs allowed, for the first time, for unique and detailed insight into the structures of heme active site of heme protein in the functional living cell. The RR spectra of physiologically important metHb, deoxyHb and oxyHb in erythrocytes were compared with the corresponding spectra of isolated proteins and revealed that the high ordering and tight packing oh Hb in cells has very little effect on the structure of heme, however some slight changes were observed in the region where vinyl bending modes are usually seen. The RR spectra indicated that the vinyl groups in the ferric and ferrous states of Hb adopt more out-of-plane conformation when the protein is enclosed in RBCs. On the other hand, the vinyl groups of $oxyHb_{RBCs}$ become more in-plane with heme macrocycle as compared to the isolated oxygenated protein. Interestingly the analysis of the spectral patterns of the oxygenated proteins and their isotopically labeled analogues revealed lack of any changes in the disposition of the Fe-O-O fragment, e.g., the frequencies and isotopic shifts of the ν(Fe—O) stretching mode in the isolated and enclosed proteins are the same. Collectively, these data indicate that the small changes in the geometry of the heme vinyl groups might be responsible for the differences in activity and ligand affinity between free Hb protein and Hb molecules enclosed within RBCs. Furthermore, these findings highlights importance of isolated protein-based studies as crucial source of information of structure – function relationship in heme protein research and opens new venues of studying these systems in functional living cells.

CRediT authorship contribution statement

Jakub Dybas: Methodology, Investigation, Formal analysis, Writing - original draft, Data curation, Funding acquisition. **Matthew J. Bokamper:** Methodology, Investigation. **Katarzyna M. Marzec:**

Supervision, Writing - review & editing, Funding acquisition. **Piotr J. Mak:** Resources, Conceptualization, Supervision, Writing - review & editing, Funding acquisition.

Declaration of competing interest

The authors declare no conflict of interest.

Acknowledgements

This work was supported by the start-up funds from Saint Louis University (P.J. Mak) and the National Science Centre, Poland (UMO 2016/23/B/ST4/00795) to K.M. Marzec. J. Dybas would like to thank the National Science Centre, Poland for financial support (UMO-2017/24/T/ST4/00452).

References

[1] K. Kaushansky, M.A. Lichtman, J.T. Prchal, M. Levi, O.W. Press, L.J. Burns, M.A. Caligiuri, Hematology, 9th ed. McGraw-Hill Education, New York, 2016.
[2] C.G. Atkins, K. Buckley, M.W. Blades, R.F.B. Turner, Raman spectroscopy of blood and blood components, Appl. Spectrosc. 71 (2017) 767–793, https://doi.org/10.1177/0003702816686593.
[3] C. Thomas, A.B. Lumb, Physiology of haemoglobin, Contin. Educ. Anaesthesia, Crit. Care Pain. 12 (2012) 251–256, https://doi.org/10.1093/bjaceaccp/mks025.
[4] R.A. Harvey, Lippincott's Illustrated Reviews, Lippincott Williams & Wilkins, 2011.
[5] B.J. Reeder, The redox activity of hemoglobins: from physiologic functions to pathologic mechanisms, Antioxid. Redox Signal. 13 (2010) 1087–1123, https://doi.org/10.1089/ars.2009.2974.
[6] J.-A. Collins, A. Rudenski, J. Gibson, L. Howard, R. O'Driscoll, Relating oxygen partial pressure, saturation and content: the haemoglobin-oxygen dissociation curve, Breathe (Sheffield, England) 11 (2015) 194–201, https://doi.org/10.1183/20734735.001415.
[7] A.M.M. Attia, F.A.A. Ibrahim, N.A. Abd El-Latif, S.W. Aziz, S.A. Abdelmottaleb Moussa, M.S. Elalfy, Determination of human hemoglobin derivatives, Hemoglobin 39 (2015) 371–374, https://doi.org/10.3109/03630269.2015.1062775.
[8] E.M. Welbourn, M.T. Wilson, A. Yusof, M.V. Metodiev, C.E. Cooper, The mechanism of formation, structure and physiological relevance of covalent hemoglobin attachment to the erythrocyte membrane, Free Radic. Biol. Med. 103 (2017) 95–106, https://doi.org/10.1016/j.freeradbiomed.2016.12.024.
[9] J. Umbreit, Methemoglobin—it's not just blue: a concise review, Am. J. Hematol. 82 (2007) 134–144, https://doi.org/10.1002/ajh.20738.
[10] V. Jeney, G. Balla, J. Balla, Red blood cell, hemoglobin and heme in the progression of atherosclerosis, Front. Physiol. 5 (2014) 379, https://doi.org/10.3389/fphys.2014.00379.
[11] D.B. Kim-Shapiro, A.N. Schechter, M.T. Gladwin, Unraveling the reactions of nitric oxide, nitrite, and hemoglobin in physiology and therapeutics, Arterioscler. Thromb. Vasc. Biol. 26 (2006) 697–705, https://doi.org/10.1161/01.ATV.0000204350.44226.9a.
[12] C.T. Andrade, L.A.M. Barros, M.C.P. Lima, E.G. Azero, Purification and characterization of human hemoglobin: effect of the hemolysis conditions, Int. J. Biol. Macromol. (2004)https://doi.org/10.1016/j.ijbiomac.2004.05.003.
[13] A. Doctor, J.S. Stamler, Nitric oxide transport in blood: a third gas in the respiratory cycle, Compr. Physiol. 1 (2011) 541–568, https://doi.org/10.1002/cphy.c090009.
[14] I.K. Quaye, Extracellular hemoglobin: the case of a friend turned foe, Front. Physiol. 6 (2015)https://doi.org/10.3389/fphys.2015.00096.
[15] A.N. Schechter, Hemoglobin research and the origins of molecular medicine, Blood 112 (2008) 3927–3938, https://doi.org/10.1182/blood-2008-04-078188.
[16] B.R. Wood, L. Hammer, L. Davis, D. McNaughton, Raman microspectroscopy and imaging provides insights into heme aggregation and denaturation within human erythrocytes, J. Biomed. Opt. 10 (2005) 14005, https://doi.org/10.1117/1.1854678.
[17] B.R. Wood, S.J. Langford, B.M. Cooke, J. Lim, F.K. Glenister, M. Duriska, J.K. Unthank, D. McNaughton, Resonance Raman spectroscopy reveals new insight into the electronic structure of β-hematin and malaria pigment, J. Am. Chem. Soc. 126 (2004) 9233–9239, https://doi.org/10.1021/ja038691x.
[18] J. Dybas, P. Berkowicz, B. Proniewski, K. Dziedzic-Kocurek, J. Stanek, M. Baranska, S. Chlopicki, K.M. Marzec, Spectroscopy-based characterization of Hb-NO adducts in human red blood cells exposed to NO-donor and endothelium-derived NO, Analyst 143 (2018) 4335–4346, https://doi.org/10.1039/c8an00302e.
[19] K.M. Marzec, J. Dybas, S. Chlopicki, M. Baranska, Resonance Raman in vitro detection and differentiation of the nitrite-induced hemoglobin adducts in functional human red blood cells, J. Phys. Chem. B 120 (2016) 12249–12260, https://doi.org/10.1021/acs.jpcb.6b08359.
[20] J. Dybas, M. Grosicki, M. Baranska, K.M. Marzec, Raman imaging of heme metabolism: in situ in macrophages and Kupffer cells, Analyst 143 (2018) 3489–3498, https://doi.org/10.1039/c8an00282g.
[21] R.L. Sparrow, M.F. Veale, G. Healey, K.A. Payne, Red blood cell (RBC) age at collection and storage influences RBC membrane-associated carbohydrates and lectin binding, Transfusion 47 (2007) 966–968, https://doi.org/10.1111/j.1537-2995.2007.01230.x.
[22] D. Perez-Guaita, M. de Veij, K.M. Marzec, A.R.D. Almohammedi, D. McNaughton, A.J. Hudson, B.R. Wood, Resonance Raman and UV-visible microscopy reveals that conditioning red blood cells with repeated doses of sodium dithionite increases haemoglobin oxygen uptake, ChemistrySelect 2 (2017) 3342–3346, https://doi.org/10.1002/slct.201700190.
[23] K.M. Marzec, D. Perez-Guaita, M. de Veij, D. McNaughton, M. Baranska, M.W.A. Dixon, L. Tilley, B.R. Wood, Red blood cells polarize green laser light revealing hemoglobin's enhanced non-fundamental Raman modes, Chemphyschem 15 (2014) 3963–3968, https://doi.org/10.1002/cphc.201402598.
[24] K.M. Marzec, A. Rygula, B.R. Wood, S. Chlopicki, M. Baranska, High-resolution Raman imaging reveals spatial location of heme oxidation sites in single red blood cells of dried smears, J. Raman Spectrosc. 46 (2014) 76–83, https://doi.org/10.1002/jrs.4600.
[25] B.R. Wood, L. Hammer, D. McNaughton, Resonance Raman spectroscopy provides evidence of heme ordering within the functional erythrocyte, Vib. Spectrosc. 38 (2005) 71–78, https://doi.org/10.1016/j.vibspec.2005.02.016.
[26] B.R. Wood, B. Tait, D. McNaughton, Micro-Raman characterisation of the R to T state transition of haemoglobin within a single living erythrocyte, Biochim. Biophys. Acta, Mol. Cell Res. 1539 (2001) 58–70, https://doi.org/10.1016/S0167-4889(01)00089-1.
[27] D. Perez-Guaita, K.M. Marzec, A. Hudson, C. Evans, T. Chernenko, C. Matthäus, M. Miljkovic, M. Diem, P. Heraud, J.S. Richards, D. Andrew, D.A. Anderson, C. Doerig, J. Garcia-Bustos, D. McNaughton, B.R. Wood, Parasites under the spotlight: applications of vibrational spectroscopy to malaria research, Chem. Rev. 118 (2018) 5330–5358, https://doi.org/10.1021/acs.chemrev.7b00661.
[28] T.G. Spiro, T.C. Strekas, Resonance Raman spectra of heme proteins. Effects of oxidation and spin state, J. Am. Chem. Soc. 96 (1974) 338–345, https://doi.org/10.1021/ja00809a004.
[29] E.R. Henry, D.L. Rousseau, J.J. Hopfield, R.W. Noble, S.R. Simon, Spectroscopic studies of protein-heme interactions accompanying the allosteric transition in methemoglobins, Biochemistry 24 (1985) 5907–5918http://www.ncbi.nlm.nih.gov/pubmed/4084499. (Accessed 26 July 2016).
[30] B.R. Wood, D. McNaughton, Raman excitation wavelength investigation of single red blood cells in vivo, J. Raman Spectrosc. 33 (2002) 517–523, https://doi.org/10.1002/jrs.870.
[31] Z. Chen, T.W.B. Ost, J.P.M. Schelvis, Phe393 mutants of cytochrome P450 BM3 with modified heme redox potentials have altered heme vinyl and propionate conformations, Biochemistry 43 (2004) 1798–1808, https://doi.org/10.1021/bi034920g.
[32] W.D. Funk, T.P. Lo, M.R. Mauk, G.D. Brayer, R.T.A. MacGillivray, A.G. Mauk, Mutagenic, electrochemical, and crystallographic investigation of the cytochrome b5 oxidation-reduction equilibrium: involvement of asparagine-57, serine-64, and heme propionate-7, Biochemistry 29 (1990) 5500–5508, https://doi.org/10.1021/bi00475a013.
[33] T.G. Spiro (Ed.), Biological Applications of Raman Spectroscopy, John Wiley & Sons, Inc., New York, 1988.
[34] P.J. Mak, Resonance Raman spectroscopy as a structural probe of cytochrome P450 enzymatic cycle, in: K.M. Kadish, K.M. Smith, R. Guilard (Eds.), Handb. Porphyr. Sci, World Scientific Publishing Co, Singapore 2016, pp. 1–120.
[35] J. Wang, W.S. Caughey, D.L. Rousseau, Resonance Raman scattering: a probe of heme protein-bound nitric oxide, in: M. Feelisch, J.S. Stamler (Eds.), Methods Nitric Oxide Res, John Wiley & Sons, Inc., New York 1996, pp. 427–454.
[36] T.G. Spiro, A.V. Soldatova, G. Balakrishnan, CO, NO and O2 as vibrational probes of heme protein interactions, Coord. Chem. Rev. 257 (2013) 511–527, https://doi.org/10.1016/j.ccr.2012.05.008.
[37] M.F. Zhu, X.P. Ye, Y.Y. Huang, Z.Y. Guo, Z.F. Zhuang, S.H. Liu, Detection of methemoglobin in whole blood based on confocal micro-Raman spectroscopy and multivariate statistical techniques, Scanning 36 (2014) 471–478, https://doi.org/10.1002/sca.21143.
[38] I.P. Torres Filho, J. Terner, R.N. Pittman, L.G. Somera III, K.R. Ward, Hemoglobin oxygen saturation measurements using resonance Raman intravital microscopy, Am. J. Physiol. Heart Circ. Physiol. 289 (2005) 488–495, https://doi.org/10.1152/ajpheart.01171.2004.
[39] I.P. Torres Filho, J. Terner, R.N. Pittman, E. Proffitt, K.R. Ward, Measurement of hemoglobin oxygen saturation using Raman microspectroscopy and 532-nm excitation, J. Appl. Physiol. 104 (2008) 1809–1817, https://doi.org/10.1152/japplphysiol.00025.2008.
[40] S. Hu, K.M. Smith, T.G. Spiro, Assignment of protoheme resonance Raman spectrum by heme labeling in myoglobin, J. Am. Chem. Soc. 118 (1996) 12638–12646, https://doi.org/10.1021/ja962239e.
[41] E. Podstawka, P.J. Mak, J.R. Kincaid, L.M. Proniewicz, Low frequency resonance Raman spectra of isolated α and β subunits of hemoglobin and their deuterated analogues, Biopolymers 83 (2006) 455–466, https://doi.org/10.1002/bip.20573.
[42] A. Szabo, L.D. Barron, Resonance Raman studies of nitric oxide hemoglobin, J. Am. Chem. Soc. 97 (1975) 660–662, https://doi.org/10.1021/ja00836a043.
[43] M. Abe, T. Kitagawa, Y. Kyogoku, Resonance Raman spectra of octaethylporphyrinatonickel(II) and meso-deuterated and nitrogen-15 substituted derivatives. II. A normal coordinate analysis, J. Chem. Phys. 69 (1978) 4526–4534, https://doi.org/10.1063/1.436450.
[44] M. Asghari-Khiavi, A. Mechler, K.R. Bambery, D. McNaughton, B.R. Wood, A resonance Raman spectroscopic investigation into the effects of fixation and dehydration on heme environment of hemoglobin, J. Raman Spectrosc. 40 (2009) 1668–1674, https://doi.org/10.1002/jrs.2317.
[45] A. Feis, M.P. Marzocchi, M. Paoli, G. Smulevich, Spin state and axial ligand bonding in the hydroxide complexes of metmyoglobin, methemoglobin, and horseradish peroxidase at room and low temperatures, Biochemistry 33 (1994) 4577–4583, https://doi.org/10.1021/bi00181a019.